# A new route for the syntheses of coordination polymers using magnetic influence: syntheses, crystal structures and fluorescence properties

**Lei Guan,\* Ying Wang, Hongzhe Jin and Pengpeng Yin**

Liaoning Petrochemical University, Fushun, Liaoning 113001, People's Republic of China. *Correspondence e-mail: guanlei@lnpu.edu.cn

Five coordination polymers $[TM^1(absa)(H_2O)_4]_n$ and $[TM^2(absa)(bipy)(H_2O)]_n$ $[TM^1 = Zn$ (**1**), Co (**2**); $TM^2 = Zn$ (**3**), Co (**4**), Cu (**5**); $Na_2absa = 5,5'$-azobissalicylic acid disodium salt; bipy = $4,4'$-bipyride] were synthesized by solvent evaporation under a magnetic field. It is evident that magnetic fields bring significant and noticeable changes to the $absa^{2-}$ ligand orientation and the component movement behaviors to construct coordination polymers. The $absa^{2-}$ ligands bind to the metal ions in bridging coordination mode through the carboxylate groups, in addition to the bipy molecules adopting bridging modes. Photoluminescence measurements indicate that the emissions of compounds **1**–**5** are at 626, 600, 632, 658 and 682 nm in the solid state, respectively.

## 1. Introduction

The self-assembly of coordination compounds is induced by the coordination bonds between metal cations and ligands, as well as various weak intermolecular interactions, such as hydrogen bonding and $\pi$–$\pi$ interactions *etc.* (Chen & Liu, 2015; Robson, 2000; Byrne *et al.*, 2008; Leong & Vittal, 2011; Huang, 2003). The self-assembly of these components in solution can construct varied coordination polymers and form diverse topological networks with high dimensionalities (Erxleben, 2003; Ghosh & Bharadwaj, 2004; He *et al.*, 2009). However, functional groups, coordination modes, charges and acidity have great effects on the final architectures, in addition to the ligands and metal cations (Kirillov, 2011; Zaworotko, 2010; Bitzer & Kleist, 2019). Therefore, the final structrual topologies induced by the weak interactions are not always unambiguously predictable and controllable. Recently, efforts have been focused on reliable synthetic strategies with the aim of obtaining predictable architectures with unusual topologies and physical properties (Lee *et al.*, 2017; Williams *et al.*, 2007). The magnetic field acts as a special driving force. The dynamical properties of the aqueous solution and colloidal system are changed under a magnetic field (Sheibani *et al.*, 2003). Additionally, the phase equilibrium relationships between components are broken (Hermann *et al.*, 2013; Gelfgat, 1999). Therefore, the use of magnetic influence has received considerable attention and has been applied in many fields, such as nanomaterials, biomedicine, environmental protection, metallurgy and semiconductors (Lin *et al.*, 2014; Serantes *et al.*, 2018; Cépas *et al.*, 2002). It has been found that a magnetic field has unexpected effects on the crystallization behavior of drug molecules, preparation of nano-materials, growth of bulk single crystals and the processes of chemical reactions (Hermann *et al.*, 2013; Ronco & Ferraudi, 1990). Consequently, our strategy – in order to gain control of and
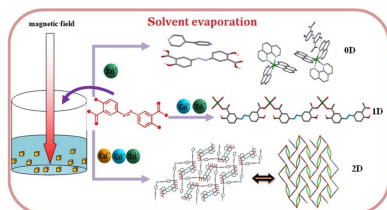
utilize the weak intermolecular interactions in solution – is to employ a controllable magnetic field as a driving force for constructing target products.

Herein, $Na_2absa$ was employed as the ligand in the design and construction of various architectures. It has three distinctive characteristics: (1) four functional groups, which can present a diverse number of potential coordination modes, allowing for the formation of diverse topologies; (2) a rigid and long molecular structure, which can give rise to the formation of interpenetrating frameworks; and (3) a $\pi$-conjugate system, which can provide a $\pi$-surface for inter-molecular interactions and can be easily affected by a magnetic field. When the $Na_2absa$ ligand was used in combi-nation with the rigid 4,4′-bipyridine (bipy) building block, five transition metal coordination polymers were synthesized via solvent evaporation under a magnetic field (see below).
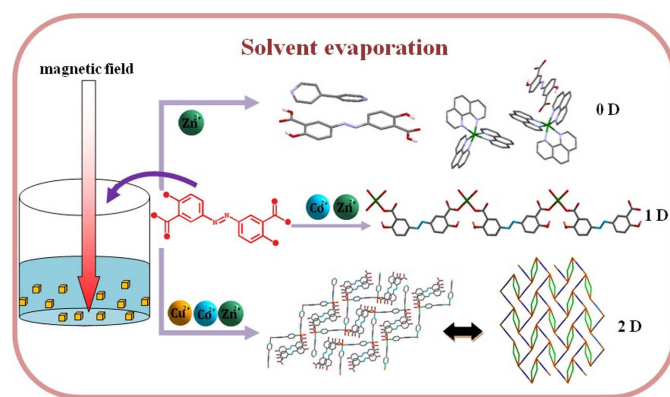


## 2. Experimental

### 2.1. Materials and general measurements

The reagents and solvents employed were commercially available and used as received without further purification. Single-crystal X-ray diffraction data were collected with a Rigaku Saturn 70 CCD, a Bruker APEX-II diffractometer or a Bruker D8 VENTURE TXS PHOTON 100 equipped with graphite monochromated Mo $K\alpha$ radiation ($\lambda$ = 0.71073 Å) using either the $\omega$ or the $\varphi$–$\omega$ scan mode. Elemental analyses of carbon, hydrogen and nitrogen were performed with a Perkin Elmer 240C elemental analyzer. The infrared spectra were measured by a Magna-IR 750 spectrophotometer in the 4000–400 cm$^{-1}$ region (KBr pellet). Thermogravimetric analyses (TGA) were carried out on a NETZSCH STA 449C unit at a heating rate of 10°C min$^{-1}$ under a nitrogen atmo-sphere. Photoluminescence analyses were performed on a Perkin Elmer LS55 fluorescence spectrometer.

### 2.2. Syntheses of $Na_2absa$ ligand

5,5′-azobissalicylic acid ($H_2absa$) was synthesized using procedures described in the literature (Kenawy et al., 2010). Sodium hydroxide solution (10%) was added dropwise to $H_2absa$ (0.302 g, 1 mmol) with stirring to a pH value of 5, and the reaction mixture was further stirred for 1 h at room temperature. The product was recrystallized three times and colorless crystals were collected by filtration and dried under vacuum at room temperature.

### 2.3. Syntheses of compounds 1 and 2

The corresponding metal nitrates (0.1 mmol) and $Na_2absa$ (0.1 mmol) were added to a vessel containing mixed solvent (5 ml of methanol and 10 ml of distilled water). The mixed solution was stirred and heated at 100°C for 3 h under a 1 T magnetic field. The solution obtained was kept in a small vial covered with parafilm at room temperature and left under a magnetic field. Block crystals were obtained after 10 days. For compound **1**, IR (KBr, cm$^{-1}$): 3023, 1579, 1479, 1448, 1328, 1248, 1187, 1079, 828, 789, 720, 577, 473. Calculated for $C_{14}H_{16}N_2O_{10}Zn$ (%): C, 38.39; H, 3.66; N, 6.40. Found (%): C, 38.42; H, 3.82; N, 6.46. For compound **2**, IR (KBr, cm$^{-1}$): 3211, 1577, 1330, 1481, 1450, 1385, 1249, 1187, 1140, 1079, 853, 826, 792, 718, 677, 626, 575, 473. Calculated for $C_{14}H_{16}N_2O_{10}Co$ (%): C, 38.96; H, 3.71; N, 6.49. Found (%): C, 38.90; H, 3.80; N, 6.55.

### 2.4. Syntheses of compounds 3–5

Compounds **3**–**5** were synthesized via a similar procedure used to produce compound **1** with the corresponding metal nitrates (0.1 mmol), $Na_2absa$ (0.1 mmol) and bipy (0.1 mmol). For compound **3**, IR (KBr, cm$^{-1}$): 3064, 1611, 1569, 1483, 1426, 1385, 1362, 1293, 1258, 1220, 1187, 1073, 832, 805, 783, 722, 642, 587, 457. Calculated for $C_{24}H_{18}N_4O_7Zn$ (%): C, 53.35; H, 3.33; N, 10.37. Found (%): C, 53.41; H, 3.40; N, 10.35. For compound **4**, IR (KBr, cm$^{-1}$): 3276, 1591, 1560, 1444, 1352, 1265, 1211, 1063, 807, 673, 630, 587, 465. Calculated for $C_{24}H_{18}N_4O_7Co$ (%): C, 52.23; H, 3.63; N, 10.16. Found (%): C, 52.20; H, 3.65; N, 10.25. For compound **5**, IR(KBr, cm$^{-1}$): 3066, 1569, 1477, 1436, 1379, 1328, 1254, 1185, 1071, 807, 681, 638, 587, 477. Calculated for $C_{24}H_{18}N_4O_7Cu$ (%): C, 53.54; H, 3.35; N, 10.41. Found (%): C, 53.57; H, 3.46; N, 10.65.

### 2.5. Crystallographic data and structure refinements

For compounds **1**, **6** and **7**, the measurement device used was a Rigaku Saturn 70 CCD; scan mode: $\omega$; data collection, cell refinement and data reduction were carried out using *CrysAlisPro* (Agilent, 2012). For compounds **2**–**4**, the measurement device was a Bruker APEX-II CCD; scan mode: $\varphi$–$\omega$; data collection was carried out using *APEX2* (Bruker, 2019); cell refinement and data reduction were carried out using *SAINT* (Bruker, 2019). For compound **5**, the measure-ment device was a Bruker D8 VENTURE TXS PHOTON 100; scan mode: $\varphi$–$\omega$; data collection was carried out using *APEX2* (Bruker, 2019); cell refinement and data reduction were carried out using *SAINT* (Bruker, 2019). For compounds **1**–**7**, the program used to solve the structure by the dual-space method was *SHELXT* (Sheldrick, 2015a) and the program used to refine the structure was *SHELXL* (Sheldrick, 2015b).

Crystallographic data were deposited in the Cambridge Crystallographic Data Centre (CCDC 2210140–2210146). The data can be obtained free of charge from https://

www.ccdc.cam.ac.uk/conts/retrieving.html or on request by
contacting deposit@ccdc.cam.ac.uk.

# 3. Results and discussion

## 3.1. Structural characterization

Single-crystal X-ray analysis reveals that compounds **1** and
**2** have similar structures, although their space groups and unit
cells are different. Therefore, only the structure of compound
**1** is described in detail. Compound **1** crystallizes in the space
group $P2_1/c$ with the monoclinic system (Table S1 of the
supporting information). The asymmetric unit comprises one
Zn atom, one absa$^{2-}$ ligand and four coordinated water
molecules [Fig. 1(a)]. Each Zn atom is in a distorted octahe-
dron [Fig. 1(b)]. The absa$^{2-}$ ligands bridge with the Zn ions to
generate a chain structure through the carboxylate groups in a
monodentate coordination fashion [Fig. 1(c)]. Note however
that both phenol groups of the absa$^{2-}$ ligand are not coordi-
nated to Zn ions which, in the protonated state, balance the
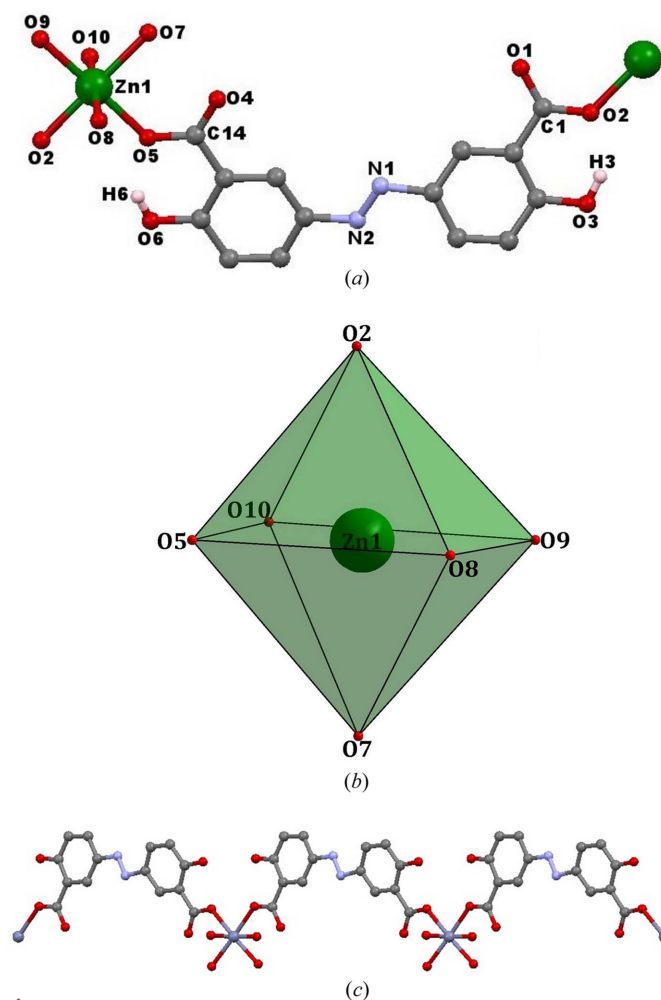charges in compound **1**.



(a)



(b)



(c)

**Figure 1**
(a) Molecular structure of compound **1** showing the atomic numbering
schemes. All hydrogen atoms, with the exception of H3 and H6, have
been omitted for clarity. (b) Coordination configuration of Zn1 ion.
(c) One-dimensional chain structure.

The structures of compounds **3–5** are similar, hence only
compound **3**, as an example, is described in detail. Single-
crystal X-ray analysis revealed that compound **3** crystallizes in
the triclinic space group $P\bar{1}$ (Table S3). Its asymmetric unit
consists of one crystallographically independent Zn atom, one
absa$^{2-}$ ligand, one bipy molecule and one coordinated water
molecule [Fig. 2(a)]. Each Zn atom adopts a distorted square-
pyramidal coordination geometry [Fig. 2(b)]. The bipy mole-
cule binds to the Zn ions, acting as a typical bridging ligand
(Table S4). Each absa$^{2-}$ ligand binds to Zn ions in bridging
mode through both monodentate carboxylate groups, leaving
both protonated phenol groups uncoordinated. Each bipy
molecule bridges with Zn ions to form a wave-like one
dimensional chain structure [Fig. 2(c)], and the absa$^{2-}$ ligands
link these one-dimensional chains to generate a two dimen-
sional network through the coordination of carboxylate
groups with Zn ions [Figs. 2(d) and 2(e)].

To gain better insight into the framework structure, a
topological analysis was carried out. Zn atoms bind to two
absa$^{2-}$ and two bipy ligands, and thus can be simplified as four-
connected nodes, with the absa$^{2-}$ and bipy ligands acting as
connecting rods. The overall topology can be described as a
four-connected framework [Fig. 2(f)]. From a topological
point of view, it exhibits a two-dimensional layered net with
the Schläfli symbol $(4^3 \cdot 6^3)$.

## 3.2. Comparison between compounds 1–5

Compounds **1–5** were synthesized by the application of a
magnetic field. Compounds **1** and **2** have similar one-dimen-
sional structures, which crystallize in the space group $P2_1/c$
with the monoclinic system, and space group $P4_32_12$ with the
tetragonal system, respectively. Compounds **3–5** have similar
two-dimensional frameworks, which crystallize in the triclinic
space group $P\bar{1}$, and monoclinic space group $P2_1/n$. Note that
their architectures are similar, but there is a slight difference in
the lattice packing. Magnetic fields can cause the interesting
phenomena observed in this work. Therefore, it is necessary to
compare the magnetic field effects in the packings and
framework geometries. As reported in the literature, on the
one hand, the presence of a magnetic field has a significant
influence on the intermolecular interactions of coordination
polymers (Zubir *et al.*, 2018). The molecules with π-conjugated
systems lie parallel to the substrate for the sample grown
under a magnetic field and slightly tilted for the sample
without a magnetic field (Kolotovska *et al.*, 2006); on the other
hand, there are noticeable changes in the morphology of
irregular agglomerates at zero field to regular crystals with
smooth surfaces under a magnetic field (Zubir *et al.*, 2016).
Therefore, in contrast to zero magnetic field, a magnetic field
can bring crystal orientation and morphology changes of
coordination polymers, and increase the symmetry of crystal
structures (Zubir *et al.*, 2018). In addition, single-crystal X-ray
analyses reveal that the average bond lengths of Zn—O and
Co—O in compounds **1** and **2** are 2.091 and 2.179 Å (Table
S2), and 2.012 Å (Zn—O) and 2.114 Å (Co—O) in
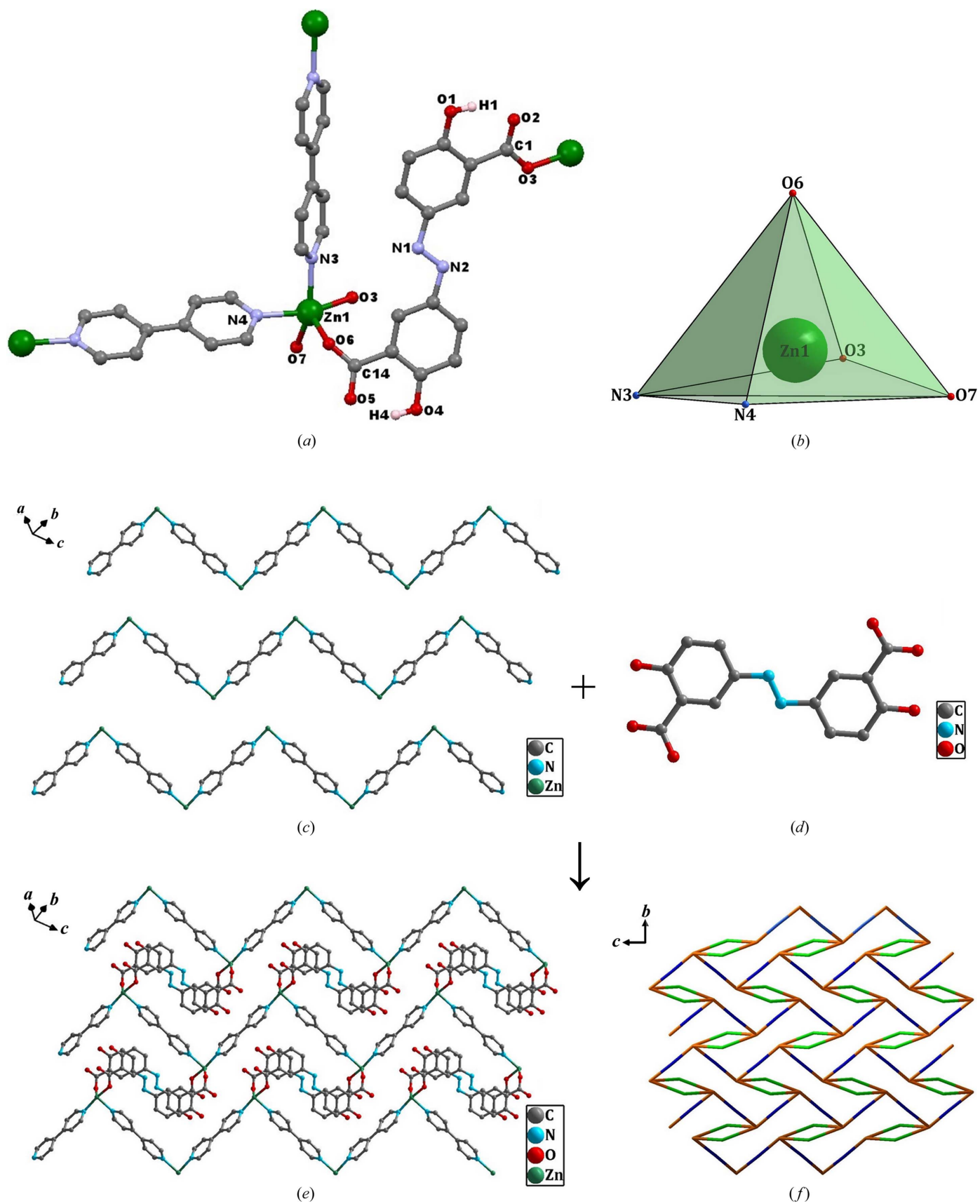compounds **3** and **4** (Table S4), respectively. Magnetic fields

**Figure 2**
(*a*) Molecular structure of compound **3** showing the atomic numbering schemes. All hydrogen atoms, with the exception of H1 and H4, have been omitted for clarity. (*b*) Coordination configuration of the Zn1 ion. (*c*) Wave-like one-dimensional chain structure based on bipy molecules and Zn ions. (*d*) Bridging absa$^{2-}$ ligand. (*e*) Two-dimensional network. (*f*) Four-connected framework.

can strengthen the bonding interaction through induction interactions (Hong *et al.*, 2019). As a consequence, Zn—O and Co—O bonds in compounds **3** and **4** are stronger than those in compounds **1** and **2**. This phenomenon may be attributed to the different interactions of the magnetic field with paramagnetic centers and antimagnetic organic molecules (Hong *et al.*, 2019), which provide an effective pathway for structural design of molecules, and even desired physical–chemical properties.

## 3.3. Influence of magnetic fields

Magnetic fields have been applied in materials research fields and achieved unexpected results (Gelfgat, 1999; Lin *et al.*, 2014; Serantes *et al.*, 2018). Introduction of a magnetic field can cause changes in magnetic orientation, mass-transport and concentration. In the preparation and self-assembly behavior, it can play an important role in increasing the directionality and collision probability of moving microparticles, and hence generate new materials (Xing *et al.*, 2009, 2007). Consequently, the morphologies, structures, sizes and properties of materials can be drastically modified, and the purity and crystallinity of materials have both shown marked improvement (Xing *et al.*, 2007; Wu *et al.*, 2005). The induction of the magnetic field is suggested to be a promising method for the preparation of novel structures. Therefore, we propose the introduction of a magnetic field into the crystal synthetic approach.

As is known, water is an important polar solvent for chemical reactions, in which electrolytes can be dissolved to form anions and cations (Li *et al.*, 2008). In solution, ligand and metal cations are affected by the thermal movement of water molecules around them, and they move and collide irregularly. Therefore, the self-assembly of ligands and metal cations was induced by the intermolecular weak interactions and coordination bonds to construct the coordinaiton compounds (Lu *et al.*, 2003). However, it is emphasized that the different structural characteristics of the coordination polymers can be mainly attributed to two main factors in this work. On the one hand, magnetic effect is essential for the well aligned orientation of aromatic ligand molecules (Morii *et al.*, 2005, 2004). In addition, a constant magnetic field influences both nucleation and growth of crystals of coordination polymers in a convection-free environment (Gavira & García-Ruiz, 2009). When the linear magnetic field is applied, the planes of the π-system in aromatic ligands are theoretically expected to orientate only perpendicular to the magnetic field in divergent directions, and the movement behaviors of metal cations and ligand anions are changed. The orientation and movement behaviors under a magnetic field can make the collision probability of the components in the specific direction much higher than other directions, which in turn affects the packing and coordination modes of the ligands with the metal cations (Li *et al.*, 2017). It would be preferable to generate crystal nucleation to grow a specific structure (Gavira & García-Ruiz, 2009). With the evaporation of the solvent, crystal nucleii can gradually precipitate from solution
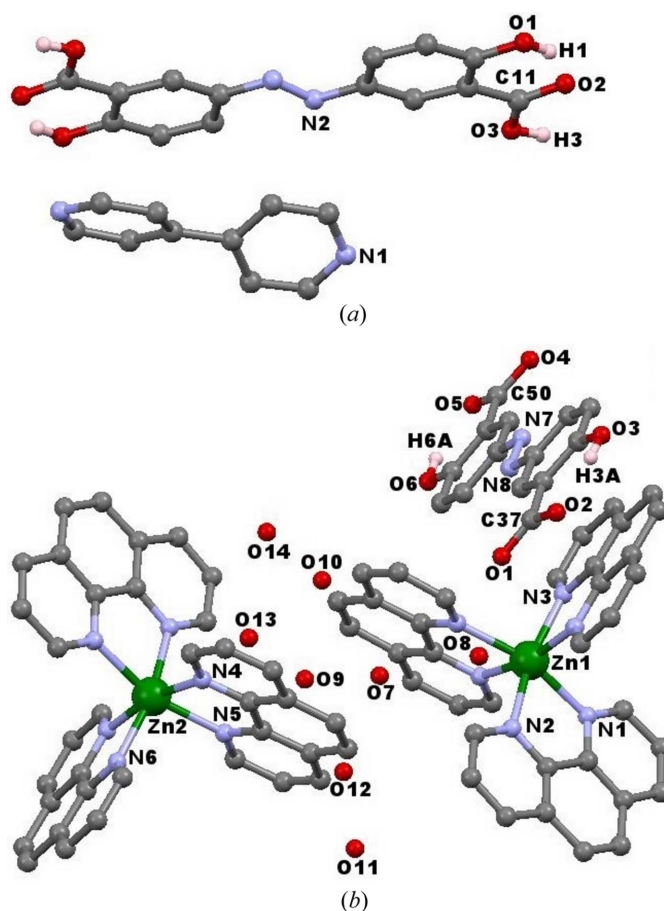


**Figure 3**
Molecular structures of (*a*) compound **6** and (*b*) compound **7** (mononuclear N-donor coordination compound) showing the atomic numbering schemes.

and grow into block crystals suitable for single-crystal X-ray diffraction.

In order to better explain the result, we conducted comparative experiments. Under zero magnetic field, (H$_2$absa)·(bipy) (**6**) is separated from the solution, where the absa$^{2-}$ ligand and bipy molecule are uncoordinated from the metal ions [Fig. 3(*a*) and Table S5]. This may be attributed to the fact that the carboxylate groups in the H$_2$absa ligand are protonated and bind to fewer metal centers.

With the increase of the magnetic field to 0.3 T, phen molecules, acting as chelated terminated ligands, prefer to coordinate with metal ions and occupy all coordination sites, in contrast to absa$^{2-}$ ligands; thus a mononuclear coordination compound with N-donor ligands [Zn(phen)$_3$]·(absa)·7H$_2$O (**7**) was obtained [Fig. 3(*b*) and Table S5]. Under a 1 T magnetic field, the absa$^{2-}$ ligands can resist irregular movement to a certain extent, and tend to be perpendicular to the magnetic field. Thus, they gain the opportunity to approach metal ions to form one-dimensional chains. When bipy is added under magnetic field, the absa$^{2-}$ ligand is perpendicular to the magnetic field, which makes the ligand coordinate with metal ions in a certain direction, generating a two-dimensional net.

Very few block crystals of compounds **1**–**5** were isolated. Many attempts were made to obtain more crystals by

improving the reaction conditions, but were unsuccessful. Because not enough samples were available, additional measurements were not performed, but thermogravimetric analyses and photoluminescence properties were studied. The effect of magnetic field on the types of structures are rather complicated and difficult to discuss. However, it is worth noting that the metal sources and the auxiliary ligands also play an important role. The orientation of the absa$^{2-}$ ligand in a magnetic field will affect its coordination mode in compounds **1** and **2** relative to compounds **6** and **7**. The presence of a high magnetic field and bipy facilitates the formation of high-dimensional coordination polymers such as compounds **3–5**. However, much more systematic work is needed to further elucidate the magnetic field effect, which can influence and induce the formation of the resultant coordination compounds. It is also anticipated that further new types of coordination polymers can be designed by this synthetic method.

### 3.4. Thermogravimetric analyses

To investigate the thermal stability of compounds **1–5**, TGA was performed under a nitrogen atmosphere at the heating rate of 10°C min$^{-1}$ between 25 and 900°C (Fig. 4). The TGA curves of compounds **1** and **2** exhibit the first weight losses of 16.7 and 16.6% in the temperature ranges 25–156°C and 25–189°C, which correspond to the release of coordinated water molecules (calculated 16.5 and 16.7%, respectively). The second weight losses in the temperature ranges 156–900°C and 189–900°C correspond to the pyrolysis of the absa$^{2-}$ ligands. Up to 900°C, the thermogravimetric curves still show downward trends. The residues may be the metal oxide. For compounds **3–5**, the weight losses in the temperature ranges 25–315°C, 25–220°C and 25–237°C amount to 3.4, 6.7 and 3.4%, which can be attributed to the removal of the coordinated water molecules (calculated 3.3, 6.5 and 3.3%, respectively). The weight losses of 29.0, 28.5 and 29.5% in the temperature ranges 315–371°C, 220–313°C and 237–280°C
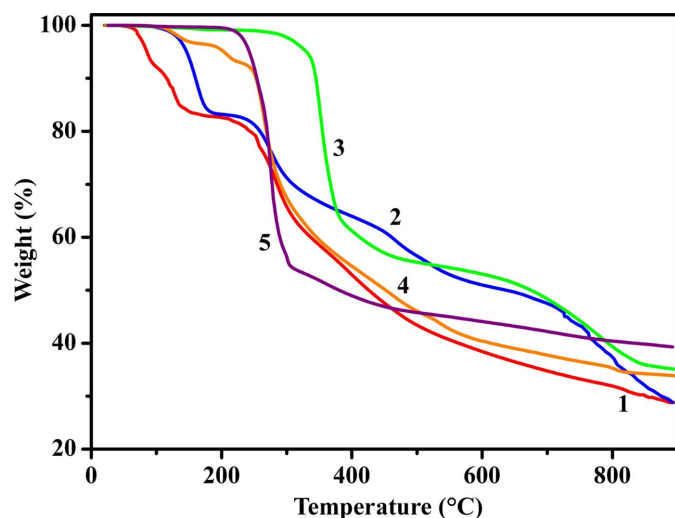


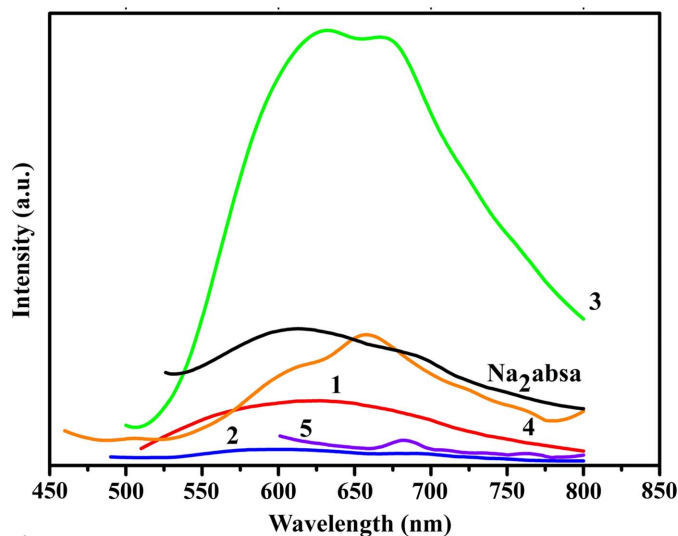**Figure 4**
TGA curves of compounds **1–5**.



**Figure 5**
Solid-state emission spectra of Na$_2$absa and compounds **1–5** at room temperature.

correspond to the loss of the bipy molecules (calculated 28.9, 28.3 and 29.0%, respectively). The weight losses in the temperature ranges 371–900°C, 313–900°C and 280–900°C correspond to the decomposing of the absa$^{2-}$ ligands. Up to 900°C, the thermogravimetric curves still show downward trends. The residues may be the metal oxide.

### 3.5. Photoluminescence properties

Luminescent coordination polymers are currently of great interest because of their applications in photochemistry, chemical sensors and luminescent displays (Allendorf *et al.*, 2009). To establish the relationship between the crystal structures and their fluorescence properties, the solid fluorescence spectra of compounds **1–5** as well as the free Na$_2$absa ligand for comparison were measured at room temperature (Fig. 5). Compounds **1–5** exhibit photoluminescence emissions at 626, 600, 632, 658 and 682 nm, respectively, which are similar to those of the free Na$_2$absa ligand with an emission maximum at 612 nm. The observed emissions in compounds **1–5** are probably caused by $\pi$–$\pi$* intra-ligand transitions of the Na$_2$absa ligand (Cheng *et al.*, 2012). The observed red and blue shifts of the emissions maximum between compounds **1–5** and the Na$_2$absa ligand were mainly attributed to the coordination of ligands with metal ions (Zhang *et al.*, 2014). However, it is found that the emission intensity of compound **3** is much higher than those of compounds **1**, **2**, **4** and **5**. This indicates that the zinc compound **3** shows better photoluminescence properties than the others. Whereas the emission intensities of compounds **1**, **2**, **4** and **5** are much lower than those of the free Na$_2$absa ligand, which indicates that the emission of the Na$_2$absa ligand was quenched to some extent.

The magnetic field assisted self-assembly based on transition metal ions and the absa$^{2-}$ ligand in the presence and absence of nitrogen donor molecules leads to the formation of coordination polymers with different characteristics. They feature one-dimensional and two-dimensional structures with

different space groups, respectively. The progressive structural characteristics result from the distinct orientation of ligands and the movement behavior of components, leading to packing in certain directions as a consequence of the effects of magnetic fields. In addition, compounds **1–5** exhibit broad fluorescent emission bands at 626, 600, 632, 658 and 682 nm, respectively.

## References

Agilent (2012). *CryAlisPRO*. Agilent Technologies Ltd, Yarnton, Oxfordshire, England.

Allendorf, M. D., Bauer, C. A., Bhakta, R. K. & Houk, R. J. T. (2009). *Chem. Soc. Rev.* **38**, 1330–1352.

Bitzer, J. & Kleist, W. (2019). *Chem. Eur. J.* **25**, 1866–1882.

Bruker (2019). *APEX2* and *SAINT*. Bruker AXS Inc., Madison, Wisconsin, USA.

Byrne, P., Lloyd, G. O., Anderson, K. M., Clarke, N. & Steed, J. W. (2008). *Chem. Commun.* pp. 3720–3722.

Cépas, O., McKenzie, R. H. & Merino, J. (2002). *Phys. Rev. B*, **65**, 100502.

Chen, X. M. & Liu, G. (2015). *Chem. Eur. J.* **8**, 4811–4817.

Cheng, P. C., Yeh, C. W., Hsu, W., Chen, T. R., Wang, H. W., Chen, J. D. & Wang, J. (2012). *Cryst. Growth Des.* **12**, 943–953.

Erxleben, A. (2003). *Coord. Chem. Rev.* **246**, 203–228.

Gavira, J. A. & García-Ruiz, J. M. (2009). *Cryst. Growth Des.* **9**, 2610–2615.

Gelfgat, Y. M. (1999). *J. Cryst. Growth*, **198–199**, 165–169.

Ghosh, S. K. & Bharadwaj, P. K. (2004). *Inorg. Chem.* **43**, 2293–2298.

He, Y. K., An, H. Y. & Han, Z. (2009). *Solid State Sci.* **11**, 49–55.

Hermann, R., Gerbeth, G. & Priede, J. (2013). *Eur. Phys. J. Spec. Top.* **220**, 227–241.

Hong, D. L., Luo, Y. H., He, X. T., He, C., Zheng, Z. Y., Su, S., Wang, C., Wang, J. Y., Chen, C. & Sun, B. (2019). *J. Phys. Chem. C*, **123**, 15230–15235.

Huang, L. M. (2003). *Microporous Mesoporous Mater.* **58**, 105–114.

Kenawy, E. R., el-R, , Al-Deyab, S. S. & El-Newehy, M. H. (2010). *Molecules*, **15**, 2257–2268.

Kirillov, A. M. (2011). *Coord. Chem. Rev.* **255**, 1603–1622.

Kolotovska, V., Friedrich, M., Zahn, D. R. T. & Salvan, G. (2006). *J. Cryst. Growth*, **291**, 166–174.

Lee, E., Seo, S., Lee, S. S. & Lindoy, L. F. (2017). *Coord. Chem. Rev.* **348**, 121–170.

Leong, W. L. & Vittal, J. J. (2011). *Chem. Rev.* **111**, 688–764.

Li, H. X., Xiong, M. W., Zhang, F., Huang, J. L. & Chai, W. (2008). *J. Phys. Chem. C*, **112**, 6366–6371.

Li, J. X., Wang, Y. J., Wei, Q. P., Xie, Y. N., Long, H. Y., Deng, Z. J., Ma, L., Yu, Z. M., Jiang, Y. L., Hu, N. X. & Zhou, K. (2017). *Surf. Coat. Technol.* **324**, 413–418.

Lin, D., Deng, B. W., Sassman, S. A., Hu, Y. W., Suslov, S. & Cheng, G. J. (2014). *RSC Adv.* **4**, 18621–18626.

Lu, T. B., Xiang, H., Luck, R. L., Mao, Z. W., Chen, X. M. & Ji, L. (2003). *Inorg. Chim. Acta*, **355**, 229–241.

Morii, N., Kido, G., Konakahara, T. & Morii, H. (2005). *Biomacromolecules*, **6**, 3259–3266.

Morii, N., Kido, G., Suzuki, H., Nimori, S. & Morii, H. (2004). *Biomacromolecules*, **5**, 2297–2307.

Robson, R. (2000). *J. Chem. Soc. Dalton Trans.* pp. 3735–3744.

Ronco, S. & Ferraudi, G. (1990). *J. Chem. Soc. Dalton Trans.* pp. 887–889.

Serantes, D., Chantrell, R., Gavilán, H., Morales, M. D. P., Chubykalo-Fesenko, O., Baldomir, D. & Satoh, A. (2018). *Phys. Chem. Chem. Phys.* **20**, 30445–30454.

Sheibani, H., Dost, S., Sakai, S. & Lent, B. (2003). *J. Cryst. Growth*, **258**, 283–295.

Sheldrick, G. M. (2015*a*). *Acta Cryst.* A**71**, 3–8.

Sheldrick, G. M. (2015*b*). *Acta Cryst.* C**71**, 3–8.

Williams, K. A., Boydston, A. J. & Bielawski, C. W. (2007). *Chem. Soc. Rev.* **36**, 729–744.

Wu, M. Z., Xiong, Y., Jia, Y. S., Niu, H. L., Qi, H. P., Ye, J. & Chen, Q. (2005). *Chem. Phys. Lett.* **401**, 374–379.

Xing, G., Jia, S. L. & Shi, Z. (2007). *Carbon*, **45**, 2584–2588.

Xing, G., Jia, S. L. & Shi, Z. Q. (2009). *Carbon*, **47**, 2112–2142.

Zaworotko, M. J. (2010). *J. Am. Chem. Soc.* **132**, 7821–7821.

Zhang, K. L., Zhong, Z. Y., Zhang, L., Jing, C. Y., Daniels, L. M. & Walton, R. I. (2014). *Dalton Trans.* **43**, 11597–11610.

Zubir, M., Hamasaki, A., Iiyama, T., Ohta, A., Ohki, H. & Ozeki, S. (2016). *Chem. Lett.* **45**, 362–364.

Zubir, M., Nasution, H. I. & Sudarma, T. F. (2018). *Russ. J. Appl. Chem.* **91**, 1867–1873.